Numerical analysis of heat conduction problems on irregular domains by means of a collocation meshless method

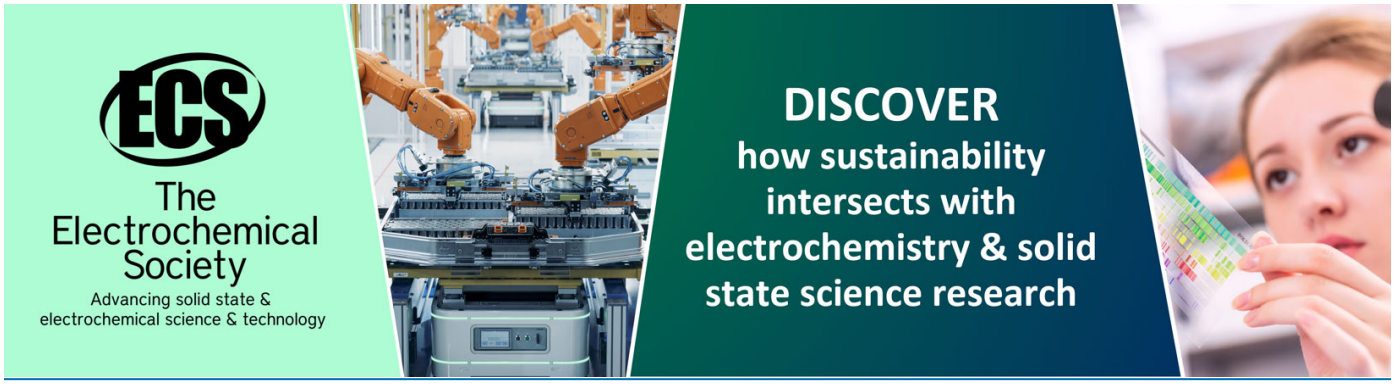

IOP Conf. Series: Journal of Physics: Conf. Series **796** (2017) 012006 doi:10.1088/1742-6596/796/1/012006

Numerical analysis of heat conduction problems on irregular domains by means of a collocation meshless method

R Zamolo and E Nobile

Dipartimento di Ingegneria e Architettura, Università degli Studi di Trieste, via A. Valerio 10, 34127 Trieste, Italy

E-mail: nobile@units.it

Abstract. A Least Squares Collocation Meshless Method based on Radial Basis Function (RBF) interpolation is used to solve steady state heat conduction problems on 2D polygonal domains using MATLAB® environment. The point distribution process required by the numerical method can be fully automated, taking account of boundary conditions and geometry of the problem to get higher point distribution density where needed. Several convergence tests have been carried out comparing the numerical results to the corresponding analytical solutions to outline the properties of this numerical approach, considering various combinations of parameters. These tests showed favorable convergence properties in the simple cases considered: along with the geometry flexibility, these features confirm that this peculiar numerical approach can be an effective tool in the numerical simulation of heat conduction problems.

1. Introduction

The accuracy of standard numerical methods used in Computational Fluid Dynamics (CFD), such as Finite Element, Finite Volume and Spectral Element Methods among others, rely on a high quality discretization of the spatial domain. This discretization process, known as meshing, heavily affects both the overall time consumption and the accuracy of the simulation, with higher costs when dealing with problems that require continuous remeshing (moving/deformable domains); finally, meshing can't always be fully automated.

To circumvent the need of a mesh, several *meshless* approaches have been proposed [1–3]: the general idea is to employ only one set of points, distributed over the domain, to approximate the unknown field and its derivatives, without any geometrical discretization of the domain.

A wide class of meshless methods which has been the object of recent developments is the one based on Radial Basis Function (RBF) interpolation [4–7]: this technique accepts only the relative (Euclidean) distance between the points as interpolation parameters. An important distinction exists between *globally supported* RBF and *locally supported* RBF, as the former produces a fully populated interpolation matrix while the latter produces a sparse matrix. We'll focus our attention on locally supported RBF because, in general, the solution of a sparse linear system can be much more efficient than the solution of a full matrix linear system; the gain in computational efficiency is balanced by the loss of spectral convegence that is a property of some globally supported RBF [8].

The final set of equations is then obtained through a *collocation* method using a number of collocation points larger than the number of the unknowns, i.e., the resulting coefficient matrix is rectangular (and sparse); therefore the least squares solution can be efficiently computed through a QR decomposition of the matrix using the standard MATLAB® built-in routines.

Several computations are carried out considering various combinations of parameters and different types of polygonal 2D domains for a simple *Poisson* equation to outline the properties of this numerical approach, comparing the computed solution to the corresponding analytical solution. These tests showed that this method can be an effective and robust tool in the numerical simulation of heat conduction problems even in complex shaped domains.

2. Governing equation and boundary conditions

Let us consider the following 2D Poisson equation in the unknown temperature field ϕ:

$$\nabla^2 \phi = q \tag{1}$$

defined on the domain Ω; equation (1) is representative of steady state heat conduction problems with internal heat generation q, in the case of a constant $k = 1$ thermal conductivity.

For simplicity let us consider only *Dirichlet* boundary conditions (fixed temperature) along the domain boundary $\Gamma = \partial\Omega$:

$$\phi = \bar{\phi} \tag{2}$$

Since the computed solution will be compared to the corresponding analytical solution ϕ_{an}, we'll set $\bar{\phi} = \phi_{an}$; the domain Ω and the terms q and ϕ_{an} will be defined case by case.

3. Domain definition

Let us consider for simplicity a 2D simply-connected polygonal domain Ω defined by a set of vertices $\mathbf{v}_i\,,\ i = 1, \ldots, V$. The sides $\Gamma_i\,,\ i = 1, \ldots, V$ connecting a vertex to the following one (except for the last side which connects the last vertex to the first) compose the domain boundary $\Gamma = \cup\Gamma_i$.

4. Point distribution

The point distribution process is here described; since two sets of points will be needed (*field* and *collocation* points, see §5.1), in this section we'll refer to a generic distribution of points $\mathbf{x}_i^{pt},\ i = 1, \ldots, N_{pt}$, where pt stands for *point type*: for field points $pt = f$ while for collocation points $pt = c$.

4.1. Uniform distribution

First of all we create a uniform cartesian distribution of $N_{U,pt}$ points covering the whole Ω with spacing h for each of the two dimensions; any spatial shift or rotation of this distribution has negligible influence on the results. Points outside Ω or lying on Γ are discarded (inside/outside Ω test is performed using a simple but efficient horizontal right hand boundary intersection).

4.2. Thickened distributions around vertices

For each vertex $\mathbf{v}_i$ where a thickened point distribution is required, two parameters are defined: a thickening parameter $\tau_i \geq 1$ and a de-thickening factor $f_i > 0$; τ_i defines the point thickening around $\mathbf{v}_i$, while f_i defines the thickening decreasing factor from $\mathbf{v}_i$.

More precisely, if $\tau_i > 1$ we define a sequence of radii r_j:

$$r_{j+1} = r_j + \frac{h}{1 + (\tau_i - 1)\exp(-r_j^2 f_i^2)} \tag{3}$$

for $j = 0, \ldots, J$ with $r_0 = 0$ till a final radius r_J such that $(r_{J+1} - r_J)/h > 0.75$.

For each radius r_j starting from r_1 we create a uniform tangential distribution of points centered in $\mathbf{v}_i$ with angular spacing $\Delta\vartheta = r_{j+1}/r_j - 1$ such that the tangential spacing is approximately equal to the radial spacing. Again, points outside Ω or lying on Γ are discarded; the total number of points for this distribution is $N_{V,pt}$.

4.3. Boundary distribution

For each side Γ_i with length L_i and vertices $\mathbf{v}_p, \mathbf{v}_q$, we define a sequence of coordinates s_j:

$$s_{j+1} = s_j + \frac{h}{1 + (\tau_p - 1)\exp(-s_j^2 f_p^2) + (\tau_q - 1)\exp(-s_j^2 f_q^2)} \tag{4}$$

for $j = 0, \ldots, J$ with $s_0 = 0$ till a final coordinate $s_{J+1} > L_i$; normalizing s_j with respect to s_{J+1}, the boundary distribution on side Γ_i is:

$$\mathbf{x}_j^{pt} = (1 - s_j)\mathbf{v}_p + s_j \mathbf{v}_q \tag{5}$$

The total number of points for this distribution is $N_{B,pt}$ and we have $N_{pt} = N_{U,pt} + N_{V,pt} + N_{B,pt}$.

4.4. Refinement process

At this point the final distribution $\mathbf{x}_i^{pt}$ may exhibit point clustering because of the superposition of the uniform distribution and the thickened distributions around vertices; this phenomenon has to be avoided because points close to each other will produce bad conditioned interpolation matrices.

To overcome this problem we employed a simple point refinement process based on the reciprocal repulsion of points: each point is subjected to the radial repulsion force of the closest 9 points (the neighbor search is done using a simple cartesian partitioning scheme).

The repulsion force magnitude is chosen to be the following:

$$F(d) = \alpha h_c \left[4 \left(\frac{d}{h_c} \right)^2 + 1 \right]^{-2} \tag{6}$$

where d is the distance between the points, $h_c = 1/\sqrt{\rho_i}$ is the local point spacing around $\mathbf{x}_i^{pt}$ ($\rho_i \approx \#points/\Delta area$ is the local point density) and $\alpha = 0.1 \div 0.6$ is an adjustable parameter.

This refinement process is iterated typically $4 \div 10$ times over the whole point set except for the boundary points which are fixed.

5. Numerical method

5.1. Point sets

Since a least squares collocation method is employed [1, 9], two point distributions are defined: the field points $\mathbf{x}_i^f$, $i = 1, \ldots, N_f$, where the N_f temperature field unknowns ϕ_i are defined, and the collocation points $\mathbf{x}_i^c$, $i = 1, \ldots, N_c$, where the discretized version of equation (1) will be written in a collocation fashion with $N_c \geq N_f$.

5.2. RBF interpolation

RBF interpolation approximates the field ϕ around $\mathbf{x}$ through the following expansion [10]:

$$\phi(\mathbf{x}) = \sum_{i=1}^{n} a_i \varphi(\|\mathbf{x} - \mathbf{x}_i^f\|) + \mathbf{b} \cdot \mathbf{x} + c \tag{7}$$

i.e., a linear combination of RBFs φ centered at the n field points $\mathbf{x}_i^f$ plus a linear polynomial in $\mathbf{x}$. If a locally supported interpolation is chosen, only the n closest points to $\mathbf{x}$ are considered.

There are many possible choices for the RBFs φ [11, 12]; the generalized Multiquadrics (MQ) have been chosen since they seem to offer the better results if appropriate parameters are employed [8, 13–15]:

$$\varphi(r) = \left[(\varepsilon r)^2 + 1\right]^{p/2} \tag{8}$$

where ε is the *shape factor* and p is an odd integer.

The coefficients a_i, $\mathbf{b}$ and c are computed writing equation (7) for the n neighbor points $\mathbf{x}_i^f$:

$$\phi(\mathbf{x}_i^f) = \phi_i \tag{9}$$

The following additional relations are needed to get a symmetric and square local interpolation coefficient matrix $\mathbf{G}$ [10]:

$$\sum_{i=1}^{n} x_i^f a_i = 0 \quad , \quad \sum_{i=1}^{n} y_i^f a_i = 0 \quad , \quad \sum_{i=1}^{n} a_i = 0 \tag{10}$$

Collecting the n coefficients a_i and the n unknown values ϕ_i in column vectors $\mathbf{a}$ and $\boldsymbol{\phi}$, respectively, the interpolation system, in compact form, is the following:

$$\mathbf{G} \begin{Bmatrix} \mathbf{a} \\ \mathbf{b} \\ c \end{Bmatrix} = \begin{Bmatrix} \boldsymbol{\phi} \\ \mathbf{0} \end{Bmatrix} \tag{11}$$

and finally, since $\mathbf{G}$ is symmetric, we have:

$$\mathbf{a}^T = \boldsymbol{\phi}^T \mathbf{G}_a^{-1} \tag{12}$$

where $\mathbf{G}_a^{-1}$ is the upper $n \times n$ submatrix of $\mathbf{G}^{-1}$.

5.3. Least squares collocation

Defining $r_i(\mathbf{x}) := \|\mathbf{x} - \mathbf{x}_i^f\|$ and putting equation (7) into equation (1) we have:

$$\sum_{i=1}^{n} a_i \nabla^2 \varphi\big(r_i(\mathbf{x})\big) = q(\mathbf{x}) \tag{13}$$

The Laplacian L of the MQ is therefore:

$$L(r) := \nabla^2 \varphi(r) = 2p\varepsilon^2 \left[(\varepsilon r)^2 + 1\right]^{p/2-1} \left[\frac{p/2 - 1}{(\varepsilon r)^2 + 1}(\varepsilon r)^2 + 1\right] \tag{14}$$

Writing equation (13) in a generic collocation point $\mathbf{x} = \mathbf{x}_j^c$ will give:

$$\sum_{i=1}^{n} a_i L\big(r_i(\mathbf{x}_j^c)\big) = q(\mathbf{x}_j^c) \tag{15}$$

Collecting the n distances r_i in the column vector $\mathbf{r}$, equation (15) can be written as:

$$\mathbf{a}^T L\big(\mathbf{r}(\mathbf{x}_j^c)\big) = q(\mathbf{x}_j^c) \tag{16}$$

Finally, recalling $\mathbf{a}^T$ from equation (12) we have:

$$\boldsymbol{\phi}^T \mathbf{G}_a^{-1} L\big(\mathbf{r}(\mathbf{x}_j^c)\big) = q(\mathbf{x}_j^c) \tag{17}$$

Equation (17) is the final scalar equation for the generic collocation point $\mathbf{x}_j^c$; the column vector $\mathbf{G}_a^{-1} L\big(\mathbf{r}(\mathbf{x}_j^c)\big)$ contains the n coefficients of this equation.

The final system is obtained writing equation (17) for all N_c collocation points:

$$\mathbf{A}\boldsymbol{\phi} = \mathbf{q} \tag{18}$$

where $\mathbf{A}$ is the $N_c \times N_f$ coefficient matrix, $\mathbf{q}$ is the column vector of generation term q evaluated at all N_c collocation points and $\boldsymbol{\phi}$ refers to all N_f field unknowns ϕ_i.

The imposition of Dirichlet boundary conditions, equation (2), is straightforward; partitioning $\mathbf{A} = [\mathbf{A}_I \mid \mathbf{A}_B]$ and $\boldsymbol{\phi} = \{\boldsymbol{\phi}_I; \boldsymbol{\phi}_B\}$ through Internal ($N_{U,f} + N_{V,f}$) and Boundary ($N_{B,f}$) field point indexes, equation (18) becomes:

$$\mathbf{A}_I \boldsymbol{\phi}_I = \mathbf{q} - \mathbf{A}_B \boldsymbol{\phi}_B \tag{19}$$

Since $N_c > N_{U,f} + N_{V,f}$, $\mathbf{A}_I$ is a tall rectangular matrix and the solution $\boldsymbol{\phi}_I$ must be computed using a least squares solver; we employed the standard MATLAB® backslash (\) operator which, in this case, performs a QR decomposition of the matrix.

5.4. Remarks on RBF interpolation

It is known that the interpolation matrix $\mathbf{G}$, equation (11), tends to be severely ill-conditioned when small shape parameters ε are employed, or when the interpolation points are close to each other, or both [16].

To alleviate this problem we employed an improved LDL solver which takes advantage of the form of the upper $n \times n$ entries of $\mathbf{G}$ ($g_{ij} = \varphi(r_{ij}) = 1 + m(r_{ij})$, where $m(\cdot)$ is the non-costant part of MacLaurin expansion of the RBF φ) to gain some numerical precision with no additional costs.

5.5. Error norm

The comparison between the computed solution ϕ_{comp} and the corresponding analytical solution ϕ_{an} will be done computing the following RMS error norm e:

$$e = \sqrt{\frac{1}{A(\Omega)} \int_\Omega (\phi_{comp} - \phi_{an})^2 \, d\Omega} \tag{20}$$

where $A(\Omega)$ is the area of Ω. The 2D integral in equation (20) is computed by numerical quadrature via a Delaunay triangulation of the field point set.

6. Numerical results and discussion

6.1. Test case A: uniform distribution, harmonic q

The problem is defined on a square domain $\Omega = [0, 1]^2$ and solved using only uniform distributions of points ($N_{V,f} = N_{V,c} = 0$) and $n = 9$ as number of local interpolation points.

The chosen reference solution is harmonic:

$$\phi_{an} = \sin(2\pi x) \sin(2\pi y) \tag{21}$$

and its Laplacian is therefore also harmonic:

$$q = \nabla^2 \phi_{an} = -8\pi^2 \sin(2\pi x) \sin(2\pi y) \tag{22}$$

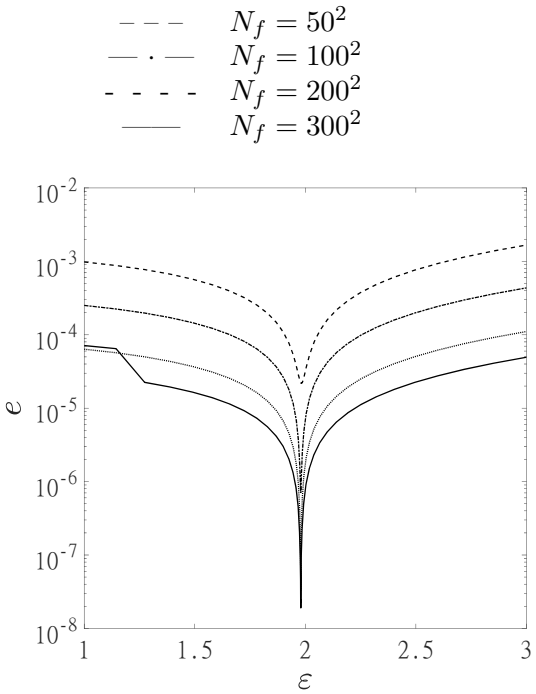

Figure 1. Test case A. Total error e versus shape parameter ε; $p = 1$ and $N_c/N_f = 2$.

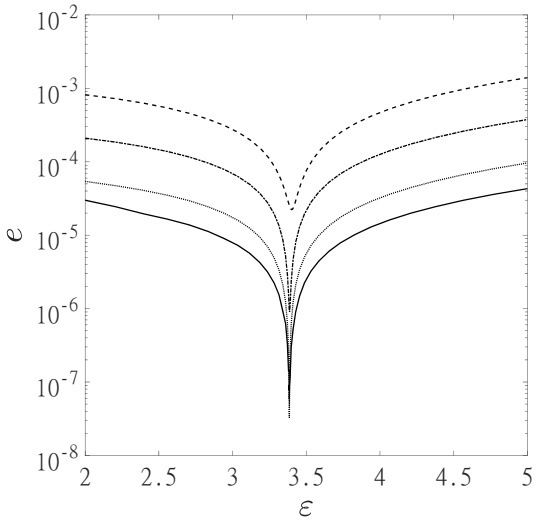

Figure 2. Test case A. Total error e versus shape parameter ε; $p = 3$ and $N_c/N_f = 2$.

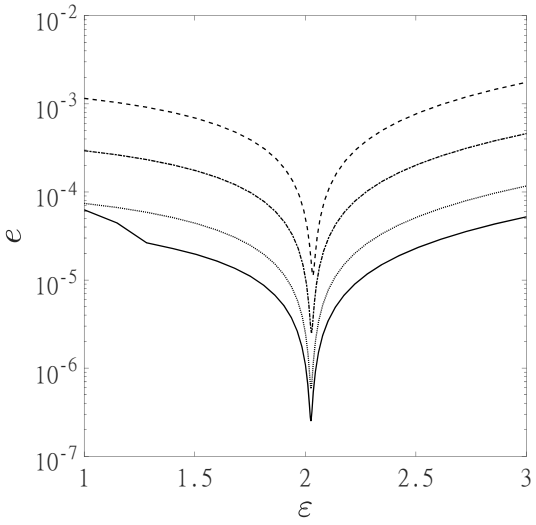

Figure 3. Test case A. Total error e versus shape parameter ε; $p = 1$ and $N_c/N_f = 4$.

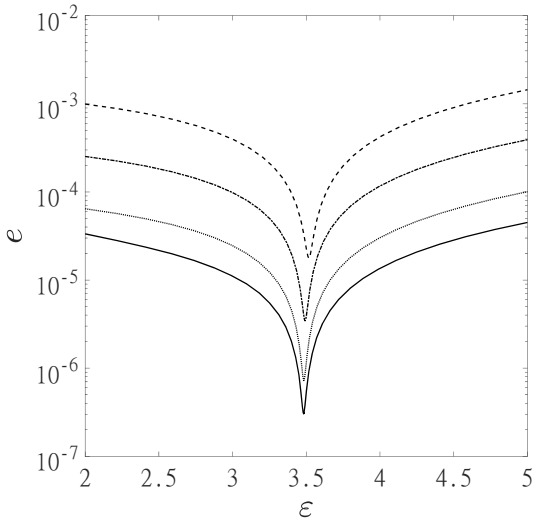

Figure 4. Test case A. Total error e versus shape parameter ε; $p = 3$ and $N_c/N_f = 4$.

First af all we investigated the influence of MQ shape parameter ε on the solution error e considering two MQ exponent factors $p = 1, 3$, two ratios $N_c/N_f = 2, 4$ and various numbers of field points N_f (Figures 1-4).

These figures show that for each MQ exponent factor p there exists a particular shape parameter ε^* which minimizes the error e; for $p = 1$, ε^* lies around 2 and for $p = 3$, ε^* lies around 3.5. However, ε^* depends upon the specific solution ϕ, so the optimal choice for ε has to be made case by case.

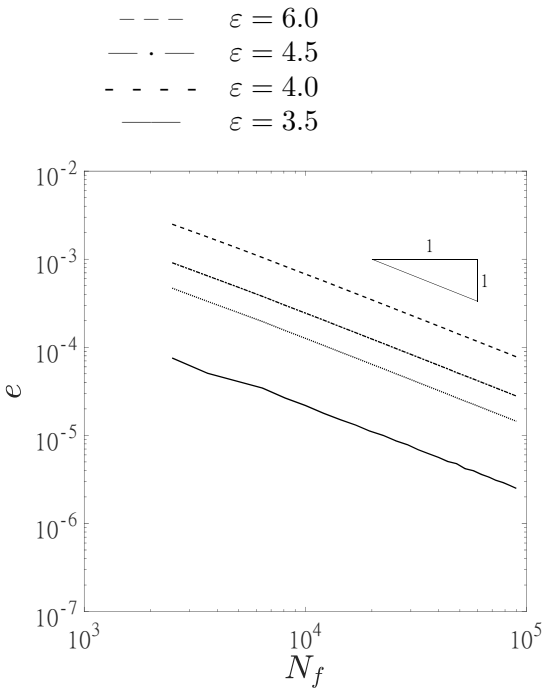

Figure 5. Test case A. Covergence curves for $p = 3$ and $N_c/N_f = 2$.

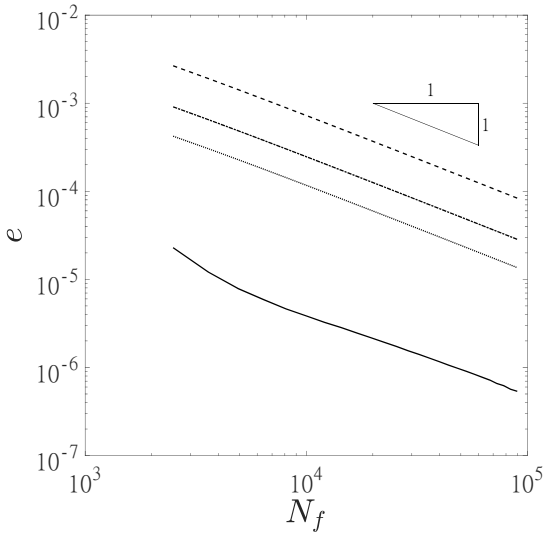

Figure 6. Test case A. Covergence curves for $p = 3$ and $N_c/N_f = 4$.

On the other hand, from the same figures it is possible to see how the influence of MQ exponent factor p is negligible on the error curves; for this reason from now on we'll consider only $p = 3$.

Finally, the influence of N_c/N_f ratio for both $p = 1$ and $p = 3$ seems to be positive on the error e only for shape parameters around ε^* but, surprisingly, the smaller error $e(\varepsilon^*)$ is observed with $N_c/N_f = 2$ instead of $N_c/N_f = 4$, i.e., employing less collocation points; for ε far from ε^*, however, this behaviour disappears.

Convergence curves for different shape parameters ε and for two ratios $N_c/N_f = 2, 4$ are reported in Figures 5 and 6. We first observe that each curve has an asymptotic slope of -1, i.e., the order of the method is 2 (in 2D the average field point spacing is $h_s \propto N_f^{-1/2}$); again, these curves clearly show that a right choice of the shape parameter ε heavily affects the error: more than two orders of magnitude of difference are observed passing from $\varepsilon = 6.0$ to $\varepsilon = 3.5$ in Figure 6.

As stated before, a comparison of previous convergence curves confirm that the influence of N_c/N_f ratio is negligible for ε far from ε^*, i.e., the upper curves (Figures 5 and 6) have similar or identical magnitude; for this reason from now on we'll consider only $N_c/N_f = 2$, as it is the cheaper choice in a computational sense.

6.2. Test case B: thickened corner, q with singularity

This problem is defined again on a square domain $\Omega = [0, 1]^2$, but both field and collocation point distributions are thickened in the corner around the $x - y$ coordinates origin $O =: \mathbf{v}_1$ ($\tau_1 > 1$), as reported in Figure 7. We employed a thickened distribution around $\mathbf{v}_1$ because the following reference solution, defined in polar coordinates, is singular in that point:

$$\phi_{an} = \sqrt{r} \tag{23}$$

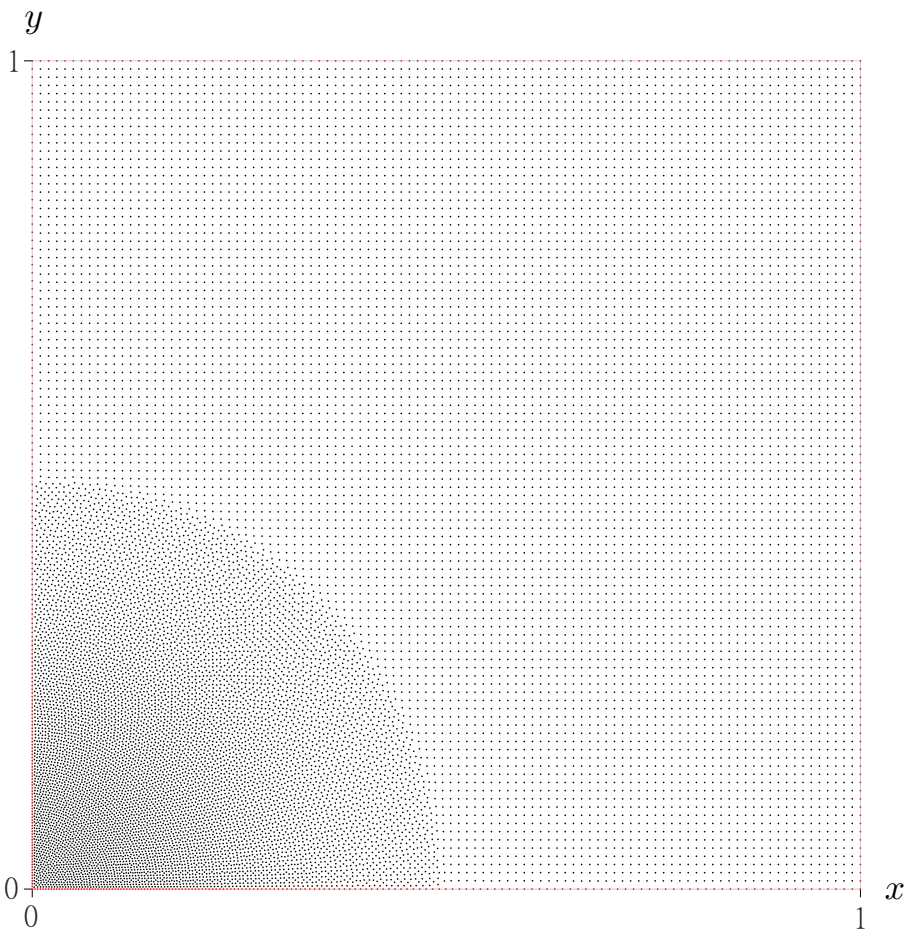

Figure 7. Field point distribution for test case B: $\tau_1 = 3.0$, $f_1 = 3.0$, $N_f = 17462$.

($r = \|\mathbf{x}\|$); its Laplacian is therefore :

$$q = \nabla^2 \phi_{an} = \frac{r^{-3/2}}{4} \tag{24}$$

The singularity of this solution is twofold: ϕ_{an} has infinite first derivatives in $\mathbf{v}_1$ and its Laplacian, which is the RHS of the problem, goes to infinity with order $3/2$ in the same point[1]; thus, this is a very severe problem. The number of local iterpolation points was again $n = 9$.

No ε^* test has been conducted in this case, thus convergence curves of Figures 8-9 have been computed only for two distinct shape factors $\varepsilon = 1.5, 3.5$, but various combinations of thickening parameters τ_1, f_1 have been considered.

In theses figure the convergence curves for a uniform point distribution are also shown; the comparison of the thickened distribution curves with the uniform distribution ones clearly reveals that in this case the employment of a thickened distribution around the singularity allows a much better resolution of the singular problem, maintaining a second order accuracy.

The influence of point distribution thickening parameters τ_1, f_1 around $\mathbf{v}_1$ is also visible in the same Figures (8-9); despite their little influence, it can be appreciated how an increase in τ_1

[1] The q term for the boundary collocation point $\mathbf{x}_k^c$ lying on the corner $\mathbf{v}_1$, where the Laplacian is infinite, should be corrected as $q_k = (h/2\tau_1)^{-3/2}$.

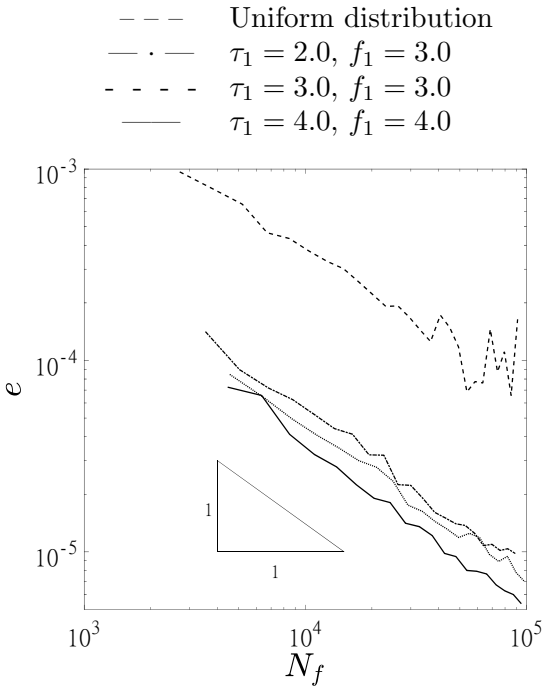

Figure 8. Test case B. Convergence curves for $\varepsilon = 1.5$.

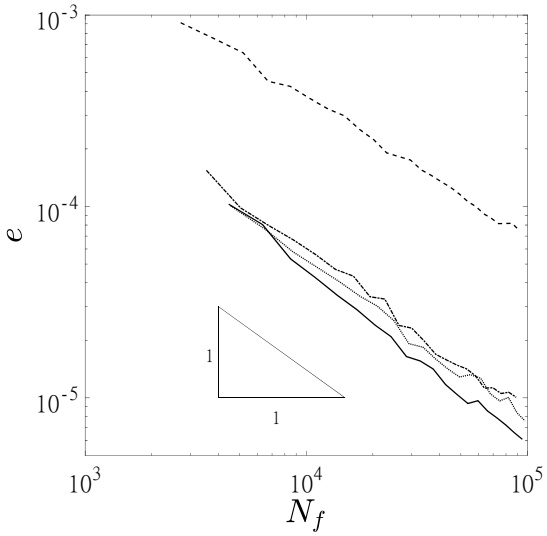

Figure 9. Test case B. Convergence curves for $\varepsilon = 3.5$.

and f_1, i.e., a thicker and localized distribution around the corner, helps in the resolution of the singularity.

Finally, the influence of shape factor ε (Figures 8-9) seems not to be of primary importance in this case, but other computations should be performed to confirm this fact; however, greater shape parameters ε reduce the ill-conditioning problems [16] when dealing with finest point distributions (i.e. high N_f / large thickening parameters τ_i).

6.3. Test case C: irregular domain, q with singularities

This problem is defined on the polygonal domain reported in Figure 11 with thickened point distributions around vertices $\mathbf{v}_2$ ($\tau_2 = 3.0, f_2 = 6.0$), $\mathbf{v}_8$ ($\tau_8 = 2.5, f_8 = 12.0$) and $\mathbf{v}_9$ ($\tau_9 = 2.5, f_9 = 12.0$). These vertices correspond to the points where the following reference solution is singular:

$$\phi_{an} = \|\mathbf{x} - \mathbf{v}_2\| + \frac{1}{4}\left(\|\mathbf{x} - \mathbf{v}_8\| + \|\mathbf{x} - \mathbf{v}_9\|\right) \tag{25}$$

Its Laplacian is therefore :

$$q = \nabla^2 \phi_{an} = \frac{1}{\|\mathbf{x} - \mathbf{v}_2\|} + \frac{1}{4}\left(\frac{1}{\|\mathbf{x} - \mathbf{v}_8\|} + \frac{1}{\|\mathbf{x} - \mathbf{v}_9\|}\right) \tag{26}$$

This reference solution is less severe than the one of test case B because ϕ_{an} has finite first derivatives, but its Laplacian goes to infinity with order 1 in the three vertices $\mathbf{v}_2, \mathbf{v}_8$ and $\mathbf{v}_9$[2].

[2] The q term for the three boundary collocation points corresponding to these three vertices $\mathbf{v}_k$, where the Laplacian is infinite, should be corrected as $q = 2a_k(h/2\tau_k)^{-1}$, with a_k the respective coefficient as in (26).

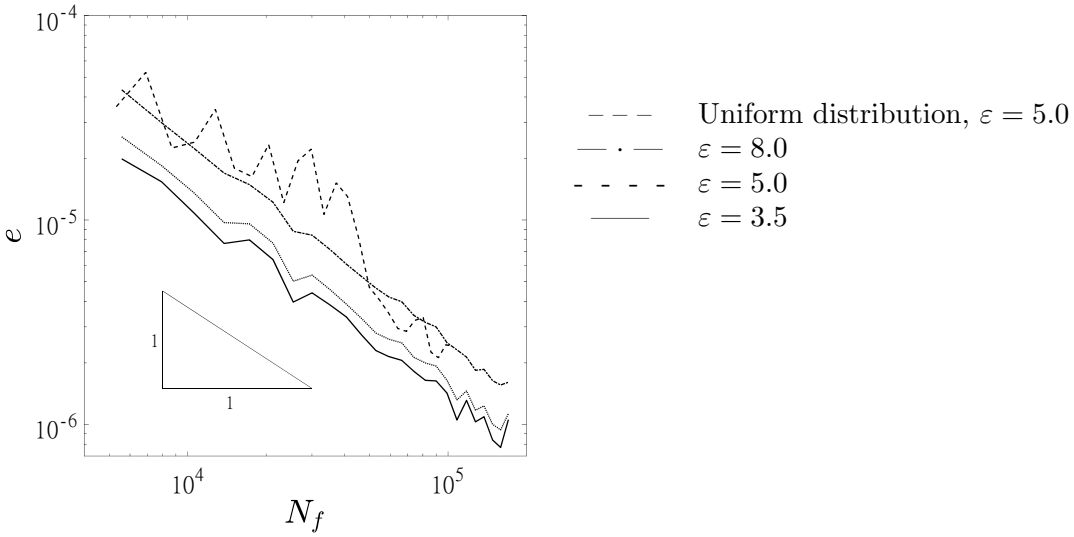

Figure 10. Test case C. Convergence curves for complex shaped domain of Figure 11.

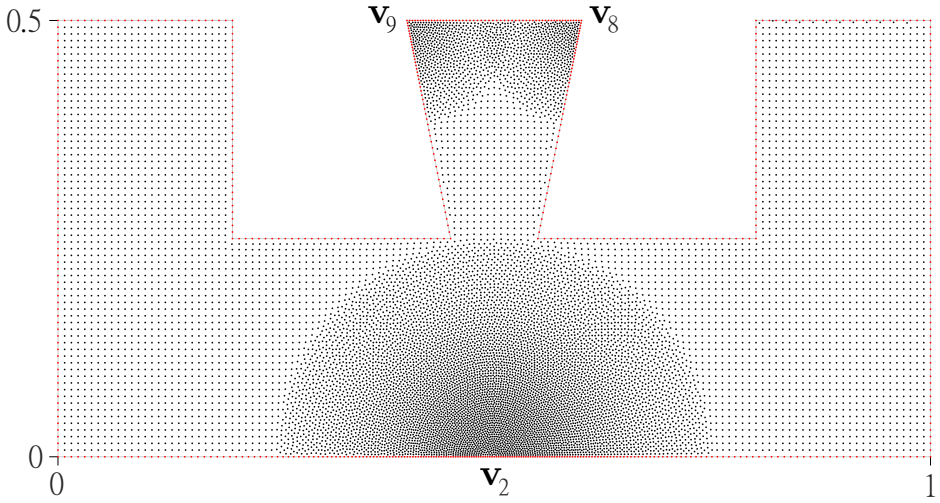

Figure 11. Field point distribution for test case C: $N_f = 13793$.

Again, $n = 9$ neighbor interpolation points are employed. Convergence curves are shown in Figure 10, where the convergence curve for a uniform distribution ($\varepsilon = 5.0$) is also reported for comparison; three shape factors $\varepsilon = 3.5, 5.0$ and 8.0 are considered.

From the previous Figure (10) it can be observed how, again, the lowering of shape factor ε reduces the total error e, maintaining a second order accuracy; this is observed at least till $N_f = 10^5$, beyond which the use of small ε (3.5,5.0) with fine point distribution causes ill-condition instabilities.

The advantage in the use of a thickened point distribution around singolarities is not so evident in this case, although some improvement exists; this little difference is due to the less severe singularities employed in this test case.

6.4. CPU times

Typical CPU time for a single complete computation, including point distribution processes, coefficients computation (requiring a space partitioning scheme with associated data structures) and least square solution (MATLAB® built-in solver), was in the order of seconds even for the cases where large number of points were employed ($N_f \approx 10^5$, $N_c \approx 4 \cdot 10^5$) on a modern laptop (quad-core Intel® i7 2.6GHz).

7. Conclusions and future work

In this work a Least Squares Collocation Meshless Method is used for the numerical simulation of heat transfer problems, in the specific case of 2D steady state conduction. The peculiarity of this approach is the flexibility against complex shaped domains because the traditional mesh/grid is no longer required.

Three particular test cases have been considered and for each test case several convergence curves have been computed to highlight the numerical properties of this approach. Each test showed good convergence properties (second order in space), even when dealing with singular data and irregular domains; in these cases thickened point distributions around singularities have been employed to improve the solution.

These numerical properties confirm that this method is an efficient and versatile tool for the numerical simulation of practical heat conduction problems in complex shaped domains.

The reported activity will be carried on in order to outline advantages and disadvantages of this specific approach for a wider range of cases. Further analyses will be conducted considering other domain geometries (not necessarily polygonal, 3D), various boundary conditions and transient (unsteady) problems; a significant step from a computational efficiency point of view will be a parallel Graphics Processing Unit (GPU) implementation of the procedure, currently under study.

References

[1] Li H and Mulay S 2013 *Meshless Methods and Their Numerical Properties* (CRC Press)
[2] Belytschko T, Krongauz Y, Organ D, Fleming M and Krysl P 1996 *Computer Methods in Applied Mechanics and Engineering* **139**(1–4) 3–47
[3] Katz A 2009 *Meshless methods for computational fluid dynamics* Ph.D. thesis Stanford University
[4] Fasshauer G 1997 *In: Surface Fitting and Multiresolution Methods* ed Mehaute A L, Rabut C and Schumaker L (Vanderbilt University Press) pp 131–138
[5] Sarler B and Vertnik R 2006 *Computers and Mathematics with Applications* **51**(8) 1269–1282
[6] Zerroukat M, Power H and Chen C 1998 *Numerical Methods in Engineering* **42**(7) 1263–1278
[7] Lai S, Wang B and Duan Y 2010 *Progress in Electromagnetics Research B* **24** 351–367
[8] Sarra S A and Kansa E 2009 *Multiquadric Radial Basis Function Approximation Methods for the Numerical Solution of Partial Differential Equations* (*Advances in Computational Mechanics* vol 2) ed Atluri S N (Tech Science Press)
[9] Zhang X, Liu X, Song K and Lu M 2001 *Numerical Methods in Engineering* **51**(9) 1089–1100
[10] Golberg M, Chen C and Bowman H 1999 *Engineering Analysis with Boundary Elements* **23**(4) 285–296
[11] Larsson E and Fornberg B 2003 *Computers and Mathematics with Applications* **46**(5–6) 891–906
[12] Hu H, Li Z and Cheng A 2005 *Computers and Mathematics with Applications* **50**(1-2) 289–320
[13] Franke R 1982 *Mathematics of Computation* **38**(157) 181–200
[14] Kansa E 1990 *Computers and Mathematics with Applications* **19**(8-9) 127–145
[15] Kansa E 1990 *Computers and Mathematics with Applications* **19**(8-9) 147–161
[16] Fornberg B and Wright G 2004 *Computers and Mathematics with Applications* **48**(5-6) 853–867